Available online at www.sciencedirect.com
ScienceDirect
Ceramics International 38 (2012) 85–92
CERAMICS INTERNATIONAL
www.elsevier.com/locate/ceramint

A comparative study of NiO–$Ce_{0.9}Gd_{0.1}O_{1.95}$ nanocomposite powders synthesized by hydroxide and oxalate co-precipitation methods

Changsheng Ding [a,*], Kazuhisa Sato [b], Junichiro Mizusaki [b], Toshiyuki Hashida [a]

[a] *Fracture and Reliability Research Institute, Tohoku University, Sendai 980-8579, Japan*
[b] *Institute of Multidisciplinary Research for Advanced Materials, Tohoku University, Sendai 980-8577, Japan*

Received 6 May 2011; received in revised form 16 June 2011; accepted 17 June 2011
Available online 24th June 2011

Abstract

In this study, NiO–$Ce_{0.9}Gd_{0.1}O_{1.95}$ (NiO–GDC) nanocomposite powders, which were applied as anode materials of low temperature solid oxide fuel cells (SOFCs), were synthesized by hydroxide and oxalate reverse co-precipitation methods, respectively. The crystal phases, crystallite size, particle size, particle size distribution, and sintering characteristics of the synthesized NiO–GDC nanocomposite powders were investigated and compared. Results showed that the different co-precipitation methods affected strongly the synthesis and characteristics of the NiO–GDC nanocomposite powders. The NiO–GDC nanocomposite powders could be synthesized at lower temperature by the hydroxide reverse co-precipitation method, and the synthesized NiO–GDC nanocomposite powders had better sinterability. The NiO–GDC nanocomposite powders synthesized by the oxalate reverse co-precipitation method had smaller particle size and uniform particle size distribution and, however, were easy to result in crack formation in the sintered disks.

Keywords: A. Sintering; Nanocomposite powders; NiO–GDC; Co-precipitation synthesis

1. Introduction

For application in solid oxide fuel cells (SOFCs), anode materials should have good electrochemical activity to oxidize fuels, high electronic conductivity, proper microstructure and good thermal expansion compatibility with other components of SOFCs [1–3]. A cermet consisting of Ni-metal and Y_2O_3-stabilized ZrO_2 (Ni–YSZ) is widely used as an anode material in high temperature SOFCs with Y_2O_3-stabilized ZrO_2 (YSZ) electrolytes, because of its good electronic conductivity, chemical and structural stability, catalytic properties and compatibility with other materials in SOFCs [4–8]. For low temperature SOFC application, however, the activity of Ni–YSZ anode is relatively low due to the low ionic conductivity of YSZ at low temperatures. In addition, Ni–YSZ is unsuitable for operation in fuels with a high methane-to-steam ratio, because of its high activity for carbon formation as well as for the steam reforming reaction [9–12]. Therefore, conventional Ni–YSZ anodes may be unsuitable to be used as anodes of low temperature SOFCs.

Gadolinium doped ceria (GDC) has higher ionic conductivity than YSZ over the temperature range of 300–700 °C [13–15]. Ni–GDC is suggested to be suitable anode for low-temperature SOFCs. In the Ni–GDC anode, Ni acts as a catalyst for the oxidation of fuels and provides electronic conduction, while GDC mainly acts as a matrix to support the Ni and prohibits the Ni from agglomeration under operating conditions. At the same time, the GDC is also used to extend Ni–GDC–gas tripe-phase boundary (TPB) into the anode [16,17]. The electrochemical reaction for the hydrogen oxidation is directly related to the length of TPB [18–20]. Large TPB can be obtained from homogeneous and continual structure of pores, Ni and GDC fine grains. Therefore, the electrochemical performance of the Ni–GDC anode is strongly dependent on its microstructure and the distribution of Ni and GDC phases [21,22]. This in turn is closely related to the characteristics of NiO and GDC powders and the fabrication process.

Anode materials were usually prepared by mechanical mixing method [23,24], where separately prepared NiO and GDC powders were mixed and sintered to form Ni–GDC

* Corresponding author. Tel.: +81 22 795 7524; fax: +81 22 795 4311.
E-mail address: dingchsh@rift.mech.tohoku.ac.jp (C. Ding).

0272-8842/$36.00
doi:10.1016/j.ceramint.2011.06.041

cermets. This method is simple and allows for accurate chemical composition, but it is difficult to obtain uniform distribution of elements in the anode, which may result in nonhomogeneous microstructure and poor electrical performance. In order to improve anode performance, it is necessary to develop NiO–GDC composite powders which have uniform distribution of elements. Some techniques such as solution combustion process [25,26], spray pyrolysis [27], polymeric organic complex solution method [28], buffer-solution method [29] and gel-precipitation method [30] have been developed to directly synthesize NiO–YSZ composite powders. Up to now, however, little work has been done on the synthesis of NiO–GDC composite powders. Gil et al. [17] reported a polymeric organic complex solution method to synthesize NiO–GDC composite powders. However, the synthesis process, which contains four heat treatment steps is relatively complex and the synthesized NiO–GDC composite powders have larger particle size. Chemical co-precipitation method is a simple and promising process to prepare homogeneous and small-sized composite powder. The chemical co-precipitation method includes normal co-precipitation method (precipitation agent solution was added into metal ion solution) and reverse co-precipitation method (metal ion solution was added into precipitation agent solution). In the previous study, we investigated the synthesis of NiO–GDC nanocomposite powders by normal co-precipitation method [31]. In order to obtain smaller and more homogeneous NiO–GDC nanocomposite powders, in this study, the reverse co-precipitation method were used to synthesize the NiO–GDC nanocomposite powders. Here, hydroxide and oxalate reverse co-precipitation methods were adopted. The characteristics of the synthesized NiO–GDC nanocomposite powders were evaluated and compared.

2. Experimental

2.1. Synthesis of NiO–GDC nanocomposite powders

The starting materials used in the synthesis of NiO–$Ce_{0.9}Gd_{0.1}O_{1.95}$ (NiO–GDC) nanocomposite powders were $Ce(NO_3)_3{\cdot}6H_2O$ (Kanto Chemical Co., 99.99%), $Gd(NO_3)_3{\cdot}6H_2O$ (Kanto Chemical Co., 99.95%) and $Ni(NO_3)_2{\cdot}6H_2O$ (Kanto Chemical Co., 99.95%). $NH_3{\cdot}H_2O$ (Kanto Chemical Co., 97.0%), NaOH (Kanto Chemical Co., 97.0%) and oxalic acid dihydrate (Kanto Chemical Co., 99.0%) were used as precipitation agents. The NiO–GDC nanocomposite powders (NiO:GDC = 60:40 mass%) were synthesized by the following two methods.

Hydroxide reverse co-precipitation method: the appropriate proportion of $Ce(NO_3)_3{\cdot}6H_2O$, $Gd(NO_3)_3{\cdot}6H_2O$ and $Ni(NO_3)_2{\cdot}6H_2O$ were dissolved into distilled water, and continuously stirred to form a homogenous solution. The homogenous solution was then added dropwise to NaOH solution containing ammonia of 3 mol% to form precipitate with stirring. And then, the precipitate was washed with distilled water and ethanol for several times to remove the Na^+, NH^{4+} and NO_3^- ions. After washing, the precipitate was dried at 60 °C, and calcined at 200–800 °C for 1 h to form NiO–GDC nanocomposite powders.

Oxalate reverse co-precipitation method: the appropriate proportion of $Ce(NO_3)_3{\cdot}6H_2O$, $Gd(NO_3)_3{\cdot}6H_2O$ and $Ni(NO_3)_2{\cdot}6H_2O$ were dissolved into ethanol, and continuously stirred to form a homogenous solution. The homogenous solution was then added dropwise to oxalic acid solution, which was made by dissolving oxalic acid into ethanol, to form precipitate with stirring. And then, the precipitate was washed with ethanol for several times. After washing, the precipitate was dried at 60 °C, and calcined at 200–800 °C for 1 h to form NiO–GDC nanocomposite powders.

2.2. Characterization

Thermogravimetric analysis and differential thermal analysis (TG/DTA) of the dried precipitate was made on a TG-DTA analyzer (Thermplus 8120, Rigaku Co., Japan) in air with a heating rate of 10 °C/min, using alumina cup as the sample container and alpha-alumina as the reference. Phase identification of the synthesized powders was performed by X-ray diffraction (XRD, MX21, Mac Science, Japan) operating with a voltage of 40 kV and current of 40 mA using CuKα radiation (λ = 1.5406 Å). The morphology and particle size of the synthesized NiO–GDC powders were examined by transmission electron microscopy (TEM,

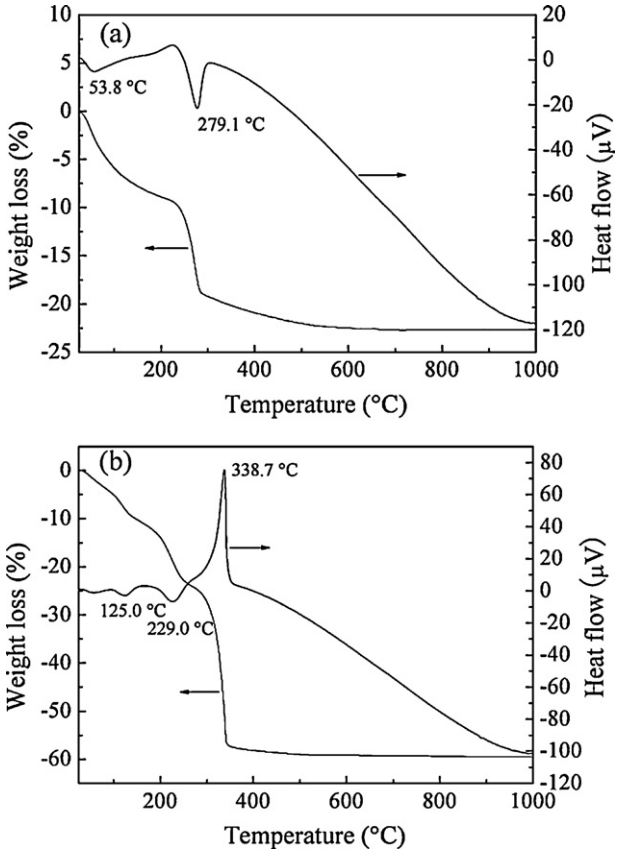

Fig. 1. TG/DTA curves of the as-prepared powders synthesized by (a) hydroxide reverse co-recipitation method and (b) oxalate reverse co-precipitation method.

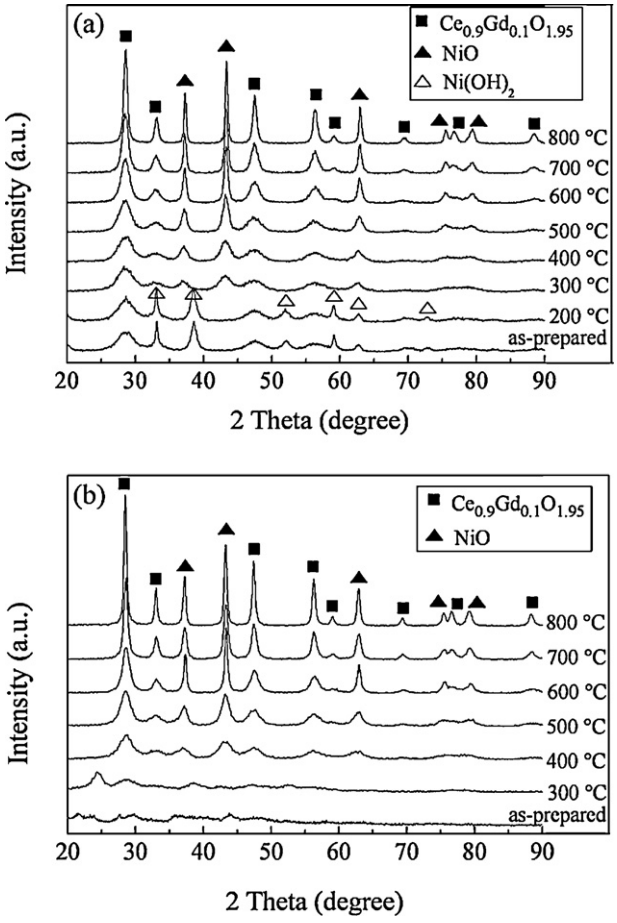

Fig. 2. XRD patterns of the NiO–GDC powders synthesized at different temperatures by (a) hydroxide reverse co-precipitation method and (b) oxalate reverse co-precipitation method.

HF-2000, Hitachi, Japan). The average particle size and particle size distribution of the synthesized NiO–GDC powders were calculated from TEM micrographs by measuring approximately 200 particles.

In order to examine the sinterability of the synthesized NiO–GDC powders, sintering experiments were performed by uniaxial pressing the NiO–GDC powders at 200 MPa to form green disks. The green disks were then sintered in air at 1100–1300 °C for 2 h. The shrinkage rate ($\Delta L/L_0$) was calculated by measuring the disk changes in length before and after sintering at different temperatures. The relative densities of the sintered disks were measured by the Archimedes method in distilled water. The microstructure of the sintered disks was observed by field-emission scanning electron microscopy (FE-SEM, S-4300, Hitachi, Japan).

3. Results and discussion

3.1. TG/DTA analysis

The TG/DTA curves of the as-prepared powders synthesized by the hydroxide and oxalate reverse co-precipitation methods are shown in Fig. 1. The total weight loss up to 600 °C is about 22.3% for the as-prepared powders synthesized by the hydroxide reverse co-precipitation method (Fig. 1a). The weight loss of about 8.8% at 25–220 °C is attributed to the removal of superficial water in the powders and crystallization water of $Ce_{0.9}Gd_{0.1}O_{1.95}{\cdot}nH_2O$. The weight loss of about 13.5% at 220–600 °C corresponds to the transition of $Ni(OH)_2$ to NiO, which is accompanied by the endothermic peak at 279.1 °C.

For the as-prepared powders synthesized by the oxalate reverse co-precipitation method, the total weight loss up to 600 °C is about 59.0% (Fig. 1b). The weight loss at 25–250 °C may be attributed to the dehydration of oxalates of cerium, gadolinium and nickel, which is accompanied by the endothermic peaks at 125 °C and 229 °C. The weight loss at 250–400 °C corresponds to the decomposition of the anhydrous oxalates and the formation of metal oxides, with the exothermic peak at 338.7 °C.

Almost no weight loss is observed above 600 °C from Fig. 1a and b, implying only the presence of NiO and GDC phases in the synthesized powders, which is further confirmed by XRD analysis.

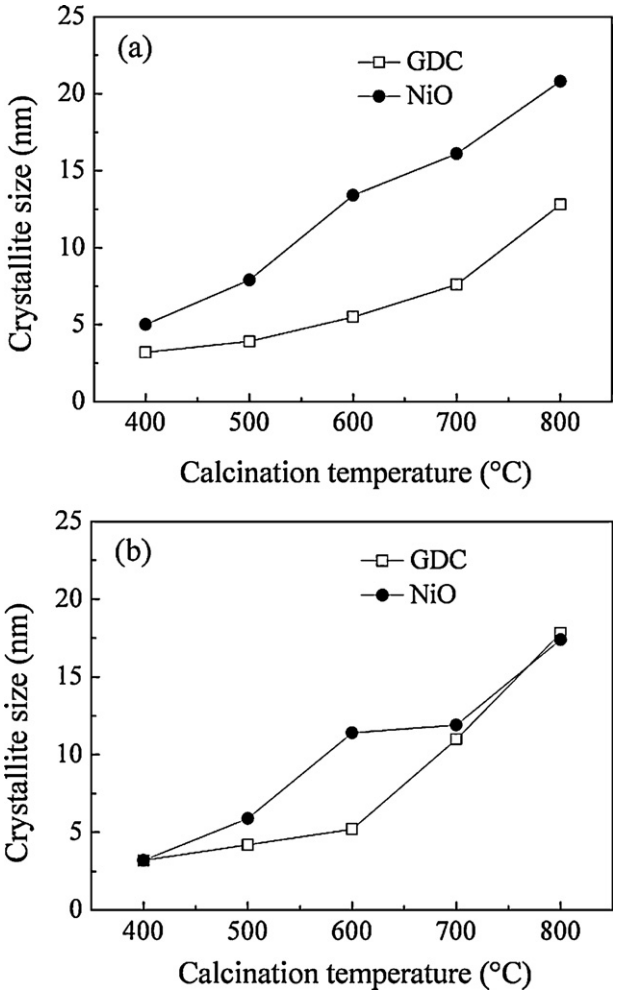

Fig. 3. Crystallite sizes of NiO and GDC phases in the NiO–GDC powders synthesized by (a) hydroxide reverse co-precipitation method and (b) oxalate reverse co-precipitation method.

3.2. XRD analysis

Fig. 2 shows the XRD patterns of the NiO–GDC powders synthesized at different temperatures by the hydroxide and oxalate reverse co-precipitation methods. It is noted that there are crystal phase peaks of $Ni(OH)_2$ and GDC in the XRD pattern of the as-prepared powders synthesized by the hydroxide reverse co-precipitation method (Fig. 2a), which means that the as-prepared powders are crystal and the GDC crystal phase has been formed in the as-prepared powders. The $Ni(OH)_2$ crystal phase begins to be converted into NiO crystal phase over 200 °C, and the transition is completed by 300 °C. This observation is in agreement with the DTA analysis (Fig. 1a). At the calcination temperature above 300 °C, the synthesized powders only consist of NiO and GDC two phases. This indicates that the NiO–GDC powders can be synthesized at 300 °C by the hydroxide reverse co-precipitation method. The change trend of crystal phases with temperature of the powders synthesized by the hydroxide reverse co-precipitation process agrees with that of the powders synthesized by the hydroxide normal co-precipitation synthesis [31], which indicates that the crystal phases of the synthesized powders are unaffected by the normal and reverse co-precipitation processes.

For the as-prepared powders synthesized by the oxalate reverse co-precipitation method, however, there is no crystal phase peaks observed in the XRD pattern (Fig. 2b), which means that the as-prepared powders are amorphous. There is GDC crystal phase observed in the powders synthesized at 300 °C. According to the DTA analysis, the decomposition of the anhydrous oxalates occurs at 250–400 °C. However, the decomposition temperature of cerium and gadolinium oxalates is lower than that of nickel oxalate. Therefore, there is no NiO crystal phase observed at 300 °C. At temperature over 300 °C, the nickel oxalate begins to be decomposed to form NiO crystal phase. At temperature above 400 °C, the synthesized powders only consist of NiO and GDC two phases. This means that the NiO–GDC powders can be synthesized at temperature above 400 °C by the oxalate reverse co-precipitation method. The synthesis temperature of the oxalate reverse co-precipitation method is higher than that of the hydroxide reverse co-precipitation method.

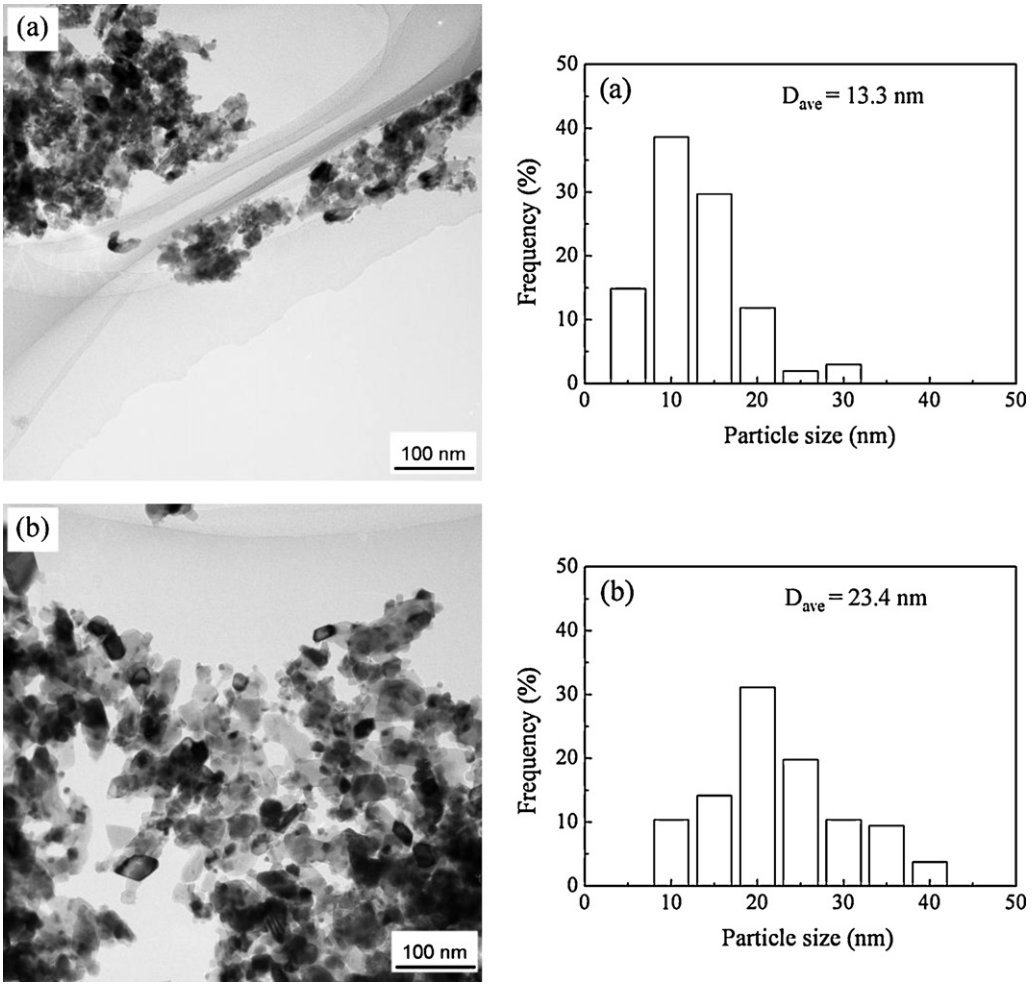

Fig. 4. TEM micrographs and particle size distribution of the NiO–GDC powders synthesized at (a) 600 °C and (b) 800 °C by hydroxide reverse co-precipitation method. D_{ave} is the average particle size.

According to the TG/DTA analysis and XRD analysis, it is concluded that the following synthesis mechanism represents the co-precipitation and calcination processes:

Hydroxide reverse co-precipitation method:

$$Ni^{2+} + OH^- \rightarrow Ni(OH)_2(Crystal) \rightarrow NiO(Crystal)$$

$$Ce^{3+} + Gd^{3+} + OH^- \rightarrow Ce_{0.9}Gd_{0.1}O_{1.95}{\cdot}nH_2O(Crystal) \rightarrow Ce_{0.9}Gd_{0.1}O_{1.95}(Crystal)$$

Oxalate reverse co-precipitation method:

$$Ni^{2+} + {C_2O_4}^{2-} \rightarrow NiC_2O_4{\cdot}nH_2O(Amorphous) \rightarrow NiO(Crystal)$$

$$Ce^{3+} + Gd^{3+} + {C_2O_4}^{2-} \rightarrow (Ce_{0.9}Gd_{0.1})_2(C_2O_4)_3{\cdot}nH_2O(Amorphous) \rightarrow Ce_{0.9}Gd_{0.1}O_{1.95}(Crystal)$$

The diffraction peaks of GDC and NiO crystal phases become sharper and more intense with an increase in the calcination temperature, which indicates a growth in the crystallite size. The crystallite sizes of GDC and NiO crystal phases were calculated from XRD lines broadening analysis according to the Scherrer equation. Fig. 3 shows the crystallite sizes of NiO and GDC crystal phases in the NiO–GDC powders synthesized at different temperatures by the hydroxide and oxalate reverse co-precipitation methods. The crystallite sizes of NiO and GDC crystal phases increase with an increase in the calcination temperature. For the NiO–GDC powders synthesized by the hydroxide reverse co-precipitation method, the crystallite size of NiO is larger than that of GDC at the same calcination temperature (Fig. 3a). This means that the NiO crystallites grow more quickly than the GDC crystallites. However, for the NiO–GDC powders synthesized by the oxalate reverse co-precipitation method, the crystallite size of NiO is only slightly larger than that of GDC at 500–700 °C (Fig. 3b). In addition, it can also be seen that the crystallite size of NiO in the NiO–GDC powders synthesized by the hydroxide reverse co-precipitation method is larger than that of NiO in the NiO–GDC powders synthesized by the oxalate reverse co-precipitation method at the same calcination temperature. The crystallite size of GDC in the NiO–GDC powders synthesized by the hydroxide reverse co-precipitation method is smaller than that of GDC in the NiO–GDC powders synthesized by the oxalate reverse co-precipitation method at the same calcination

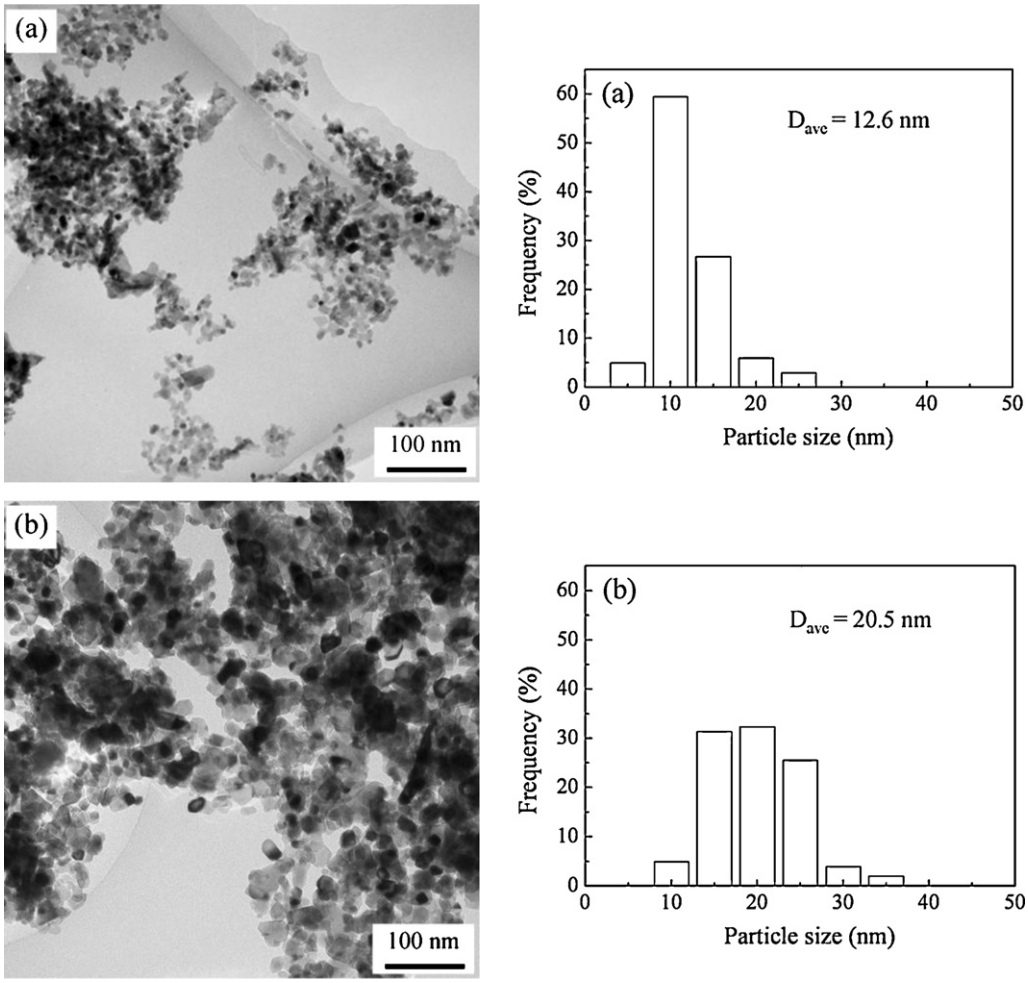

Fig. 5. TEM micrographs and particle size distribution of the NiO–GDC powders synthesized at (a) 600 °C and (b) 800 °C by oxalate reverse co-precipitation method. D_{ave} is the average particle size.

temperature above 600 °C. This indicates that the different reverse co-precipitation methods affect strongly the crystallite sizes of NiO and GDC crystal phases due to the different synthesis mechanism.

3.3. TEM observation

Figs. 4 and 5 show the TEM micrographs and particle size distribution of the NiO–GDC powders synthesized at 600 and 800 °C by the hydroxide and oxalate reverse co-precipitation methods. It can be seen that all the NiO–GDC powders synthesized by the hydroxide and oxalate reverse co-precipitation methods consist of nano-sized particles and the particle size of the NiO–GDC powders increases with an increase in the calcination temperature. The average particle sizes of the NiO–GDC nanocomposite powders synthesized at 600 and 800 °C by the hydroxide reverse co-precipitation method are 13.3 and 23.4 nm, respectively. At the same synthesis temperature, the average particle size of the NiO–GDC nanocomposite powders synthesized by the hydroxide reverse co-precipitation method is smaller than that of the NiO–GDC nanocomposite powders synthesized by the hydroxide normal co-precipitation method (16.1 nm and 36.3 nm at 600 and 800 °C, respectively) [31]. In addition, the particle size distribution of the NiO–GDC nanocomposite powders synthesized by the hydroxide reverse co-precipitation method is narrower than that of the NiO–GDC nanocomposite powders synthesized by the hydroxide normal co-precipitation method [31]. These indicate that smaller and more uniform NiO–GDC nanocomposite powders can be synthesized by the hydroxide reverse co-precipitation method.

Compared with the NiO–GDC nanocomposite powders synthesized by the hydroxide reverse co-precipitation method, the NiO–GDC nanocomposite powders synthesized by the oxalate reverse co-precipitation method have smaller average particle size and narrower particle size distribution (Fig. 5). This means that the different co-precipitation methods affect strongly the average particle size and particle size distribution of the synthesized NiO–GDC nanocomposite powders. The difference of average particle size and particle size distribution of the synthesized NiO–GDC nanocomposite powders may be attributed to the formation of crystal phases in the as-prepared powders. The crystal phases grow continuously with increasing calcination temperature, which results in the formation of larger particles.

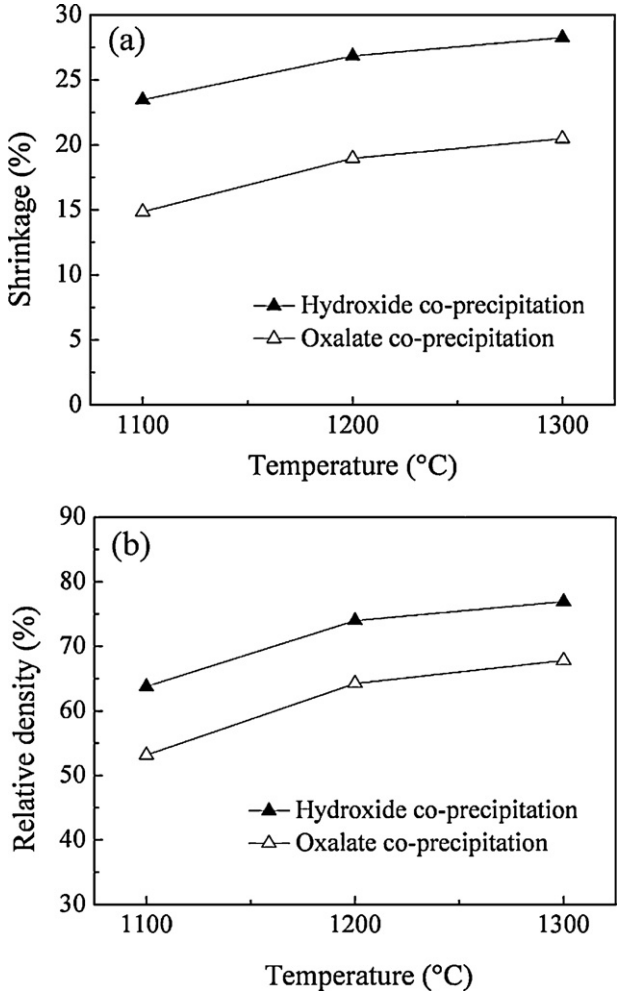

Fig. 6. Shrinkages (a) and relative densities (b) of the NiO–GDC disks prepared at different temperatures from the NiO–GDC nanocomposite powders synthesized by hydroxide reverse co-precipitation method and oxalate reverse co-precipitation method.

3.4. Sintering

Fig. 6 shows the shrinkages and relative densities of the NiO–GDC disks prepared at different temperatures from the NiO–GDC nanocomposite powders synthesized at 600 °C by the hydroxide and oxalate reverse co-precipitation methods. The NiO–GDC disks prepared from the NiO–GDC nanocomposite powders synthesized by the hydroxide reverse co-precipitation method have larger shrinkage and higher relative density than the NiO–GDC disks prepared from the NiO–GDC nanocomposite powders synthesized by the oxalate reverse co-precipitation method. This indicates that the NiO–GDC nanocomposite powders synthesized by the hydroxide reverse co-precipitation method have better sinterability than the NiO–GDC nanocomposite powders synthesized by the oxalate reverse co-precipitation method.

Fig. 7 shows the SEM micrographs of the NiO–GDC disks prepared at 1300 °C from the NiO–GDC nanocomposite powders synthesized by the hydroxide and oxalate reverse co-precipitation methods. It can be seen that the NiO–GDC disk prepared from the NiO–GDC nanocomposite powders synthesized by the hydroxide reverse co-precipitation method shows uniform microstructure without cracks, whereas there are many big cracks formed in the NiO–GDC disk prepared from the NiO–GDC nanocomposite powders synthesized by the oxalate reverse co-precipitation method. The cracks may result from the quick shrinkage of some parts of the NiO–GDC disk during sintering. It can be noted that the crack-free parts are relatively dense (Fig. 7b). Thus, it can be concluded that the formation of

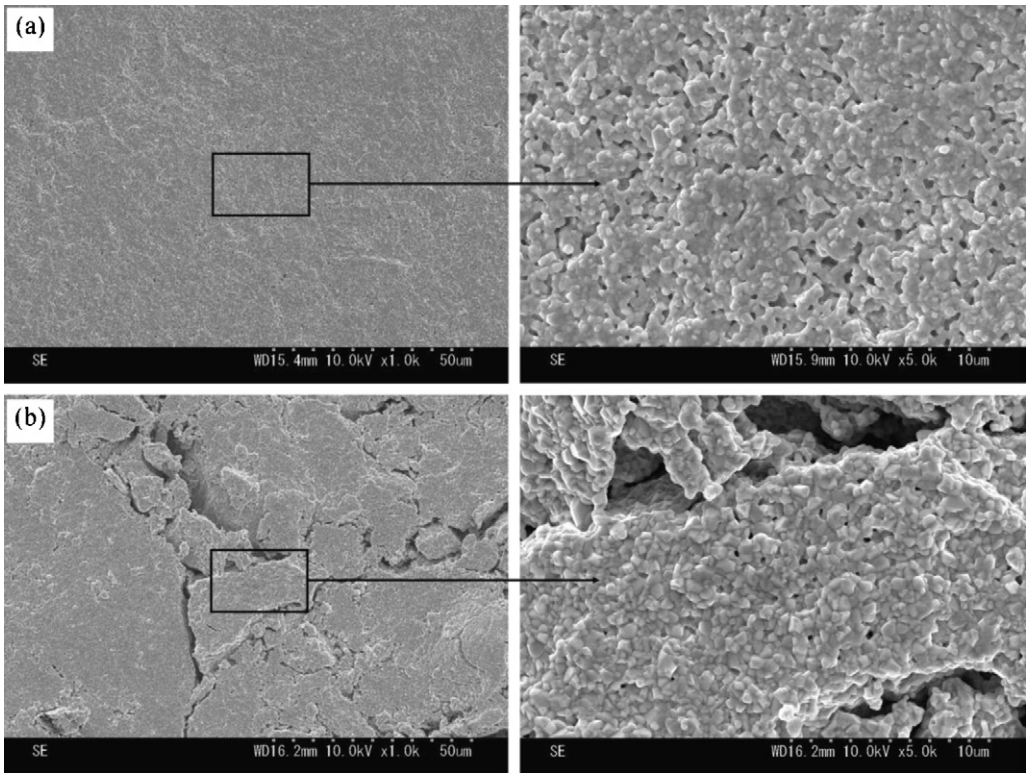

Fig. 7. SEM photographs of the NiO–GDC disks prepared at 1300 °C from the NiO–GDC nanocomposite powders synthesized by (a) hydroxide reverse co-precipitation method and (b) oxalate reverse co-precipitation method.

the cracks result in small shrinkage and low relative density of the NiO–GDC disks prepared from the NiO–GDC nanocomposite powders synthesized by the oxalate reverse co-precipitation method.

For applying in anode-supported SOFCs, the formation of cracks in anode disks is unaccepted because that the cracks decrease the mechanical strength of the anode disks and result in the difficulty in preparing dense and crack-free electrolyte films on the anode disks. Therefore, the application of the NiO–GDC nanocomposite powders synthesized by the oxalate reverse co-precipitation method need to be investigated farther.

4. Conclusions

NiO–GDC nanocomposite powders with average particle size of less than 25 nm have been successfully synthesized by hydroxide and oxalate reverse co-precipitation methods. The different co-precipitation methods affect the crystal phase formation, crystallite size, particle size and sintering characteristics of the NiO–GDC nanocomposite powders. The NiO–GDC nanocomposite powders synthesized by the oxalate reverse co-precipitation method have smaller and more uniform particles. However, the cracks are easy to be formed in the sintered NiO–GDC disks. The NiO–GDC nanocomposite powders synthesized by the hydroxide reverse co-precipitation method show better sintering characteristics.

Acknowledgements

This work was supported partly by the NEDO project, ‘‘Development of Systems and Elemental Technology on SOFC’’, and by the Japan Ministry of Education, Culture, Sports, Science and Technology under Grant-in-Aid for Scientific Research (B) (no. 18360053).

References

[1] D.W. Dees, T.D. Claar, T.E. Easler, D.C. Fee, F.C. Mrazek, Conductivity of porous Ni/ZrO_2–Y_2O_3 cermets, J. Electrochem. Soc. 134 (1987) 2141–2146.
[2] N.Q. Minh, Ceramic fuel cells, J. Am. Ceram. Soc. 76 (1993) 563–588.
[3] M. Brown, S. Primdahl, M. Mogensen, Structure/performance relations for Ni/Yttria-stabilized zirconia anodes for solid oxide fuel cells, J. Electrochem. Soc. 147 (2000) 475–485.
[4] C.H. Lee, C.H. Lee, H.Y. Lee, S.M. Oh, Microstructure and anodic properties of Ni/YSZ cermets in solid oxide fuel cells, Solid State Ionics 98 (1997) 39–48.
[5] M. Mogensen, S.P. Primdahl, M.J. Jorgensen, C. Bagger, Composite electrodes in solid oxide fuel cells and similar solid state devices, J. Electroceram. 5 (2000) 141–152.
[6] M. Radovic, E.L. Curzio, Mechanical properties of tape cast nickel-based anode materials for solid oxide fuel cells before and after reduction in hydrogen, Acta Mater. 52 (2004) 5747–5756.
[7] S.P. Jiang, S.H. Chan, A review of anode materials development in solid oxide fuel cells, J. Mater. Sci. 39 (2004) 4405–4439.
[8] G.Q. Shao, H. Cai, J.R. Xie, X.L. Guan, B.L. Wu, R.Z. Yuan, J.K. Guo, Preparation of nanocomposite Ni/YSZ cermet powder by EDTA complexes–gel conversion process, Mater. Lett. 57 (2003) 3287–3290.

[9] P. Holtappels, J. Bradley, J.T.S. Irvine, A. Kaiser, M. Mogensen, Electrochemical characterization of ceramic SOFC anodes, J. Electrochem. Soc. 148 (2001) A923–A929.
[10] R.J. Gorte, J.M. Vohs, S. Mcintosh, Recent developments on anodes for direct fuel utilization in SOFC, Solid State Ionics 175 (2004) 1–6.
[11] M.L. Toebes, J.H. Bitter, A.J. Dillen, K.P. Jong, Impact of the structure and reactivity of nickel particles on the catalytic growth of carbon nanofibers, Catal. Today 76 (2002) 33–42.
[12] S.P. Yoon, J. Han, S.W. Nam, T.H. Lim, S.A. Hong, Improvement of anode performance by surface modification for solid oxide fuel cell running on hydrocarbon fuel, J. Power Sources 136 (2004) 30–36.
[13] B.C.H. Steele, A. Heinzel, Materials for fuel-cell technologies, Nature 414 (2001) 345–352.
[14] R.S. Torrens, N.M. Sammes, G.A. Tompsett, Characterisation of $(CeO_2)_{0.8}(GdO_{1.5})_{0.2}$ synthesised using various techniques, Solid State Ionics 111 (1998) 9–15.
[15] M. Mogensen, N.M. Sammes, G.A. Tompsett, Physical, chemical and electrochemical properties of pure and doped ceria, Solid State Ionics 129 (2000) 63–94.
[16] Y. Okawa, T. Matsumoto, T. Doi, Y. Hirata, Thermal stability of nanometer-sized NiO and Sm-doped ceria powders, J. Mater. Res. 17 (2002) 2266–2274.
[17] V. Gil, C. Moure, J. Tartaj, Sinterability, microstructures and electrical properties of Ni/Gd-doped ceria cermets used as anode materials for SOFCs, J. Eur. Ceram. Soc. 27 (2007) 4205–4209.
[18] S.P. Jiang, Y.Y. Duan, J.G. Love, Fabrication of high-performance Ni/Y_2O_3–ZrO_2 cermet anodes of solid oxide fuel cells by ion impregnation, J. Electrochem. Soc. 149 (2002) A1175–A1183.
[19] B. Boer, M. Gonzalez, H.J.M. Bouwmeester, H. Verweij, The effect of the presence of fine YSZ particles on the performance of porous nickel electrodes, Solid State Ionics 127 (2000) 269–276.
[20] A. Bieberle, L.P. Meier, L.J. Gauckler, The electrochemistry of Ni pattern anodes used as solid oxide fuel cell model electrodes, J. Electrochem. Soc. 148 (2001) A646–A656.
[21] S.P. Jiang, P.J. Callus, S.P.S. Badwal, Fabrication and performance of Ni/3 mol% Y_2O_3–ZrO_2 cermet anodes for solid oxide fuel cells, Solid State Ionics 132 (2000) 1–14.
[22] Y. Okawa, Y. Hirata, Sinterability, microstructures and electrical properties of Ni/Sm-doped ceria cermet processed with nanometer-sized particles, J. Eur. Ceram. Soc. 25 (2005) 473–480.
[23] T. Ishihara, T. Shibayama, H. Nishiguchi, Y. Takita, Nickel–Gd-doped CeO_2 cermet anode for intermediate temperature operating solid oxide fuel cells using $LaGaO_3$-based perovskite electrolyte, Solid State Ionics 132 (2000) 209–216.
[24] S.W. Zha, W. Rauch, M.L. Liu, Ni–$Ce_{0.9}Gd_{0.1}O_{1.95}$ anode for GDC electrolyte-based low-temperature SOFCs, Solid State Ionics 166 (2004) 241–250.
[25] S.T. Aruna, M. Muthuraman, K.C. Patil, Synthesis and properties of Ni–YSZ cermet: anode material for solid oxide fuel cells, Solid State Ionics 111 (1998) 45–51.
[26] A. Ringuede, J.A. Labrincha, J.R. Frade, A combustion synthesis method to obtain alternative cermet materials for SOFC anodes, Solid State Ionics 141–142 (2001) 549–557.
[27] T. Fukui, S. Ohara, M. Naito, K. Nogi, Performance and stability of SOFC anode fabricated from NiO/YSZ composite particles, J. Eur. Ceram. Soc. 23 (2003) 2963–2967.
[28] P. Duran, J. Tartaj, F. Capel, C. Moure, Processing and characterisation of a fine nickel oxide/zirconia/composite prepared by polymeric complex solution synthesis, J. Eur. Ceram. Soc. 23 (2003) 2125–2133.
[29] Y. Li, Y.S. Xie, J.H. Gong, Y.F. Chen, Z.T. Zhang, Preparation of Ni/YSZ materials for SOFC anodes by buffer-solution method, Mater. Sci. Eng. B 86 (2001) 119–122.
[30] M. Marinsek, K. Zupan, J. Macek, Preparation of Ni–YSZ composite materials for solid oxide fuel cell anodes by the gel-precipitation method, J. Power Sources 86 (2000) 383–389.
[31] C.S. Ding, H.F. Lin, K. Sato, T. Hashida, Synthesis of NiO–$Ce_{0.9}Gd_{0.1}O_{1.95}$ nanocomposite powders for low-temperature solid oxide fuel cell anodes by co-precipitation, Scripta Mater. 60 (2009) 254–256.